PAPER

# Biomimetic human skin model patterned with rete ridges

Biofabrication

PAPER

# Biomimetic human skin model patterned with rete ridges

Maxwell B Nagarajan[1,2], Alexander J Ainscough[1,2], Daniel S Reynolds[1,2], Sebastien G M Uzel[1,2], Jason W Bjork[3], Bryan A Baker[3], Amy K McNulty[3], Susan L Woulfe[3,*] and Jennifer A Lewis[1,2,*]

[1] John A. Paulson School of Engineering and Applied Sciences, Harvard University, Cambridge, MA 02138, United States of America
[2] Wyss Institute for Biologically Inspired Engineering, Harvard University, Boston, MA 02115, United States of America
[3] 3M, 3M Center, St. Paul, MN 55144, United States of America
[*] Authors to whom any correspondence should be addressed.

**E-mail:** swoulfe@mmm.com and jalewis@seas.harvard.edu

**RECEIVED**
14 June 2023

**REVISED**
23 August 2023

**ACCEPTED FOR PUBLICATION**
21 September 2023

**PUBLISHED**
20 October 2023

**Keywords:** biomimetic skin model, rete ridges, epidermis, dermis, telocollagen

Supplementary material for this article is available online

## Abstract

Rete ridges consist of undulations between the epidermis and dermis that enhance the mechanical properties and biological function of human skin. However, most human skin models are fabricated with a flat interface between the epidermal and dermal layers. Here, we report a micro-stamping method for producing human skin models patterned with rete ridges of controlled geometry. To mitigate keratinocyte-induced matrix degradation, telocollagen–fibrin matrices with and without crosslinks enable these micropatterned features to persist during longitudinal culture. Our human skin model exhibits an epidermis that includes the following markers: cytokeratin 14, p63, and Ki67 in the basal layer, cytokeratin 10 in the suprabasal layer, and laminin and collagen IV in the basement membrane. We demonstrated that two keratinocyte cell lines, one from a neonatal donor and another from an adult diabetic donor, are compatible with this model. We tested this model using an irritation test and showed that the epidermis prevents rapid penetration of sodium dodecyl sulfate. Gene expression analysis revealed differences in keratinocytes obtained from the two donors as well as between 2D (control) and 3D culture conditions. Our human skin model may find potential application for drug and cosmetic testing, disease and wound healing modeling, and aging studies.

## 1. Introduction

An undulating interface exists between the epidermal and dermal layers in human skin, which enhances layer adhesion as well as skin elasticity [1, 2]. These features, known as rete ridges (or pegs), are typically 50–400 $\mu$m in width and depth [3–5]. Epidermal stem cells are typically concentrated in the tips or troughs of the rete ridges [6, 7]. When human skin is damaged by wounds, chronic disease, or aging, its rete ridge architecture flattens leading to a reduction in biomechanical function [1, 8–10]. Hence, the generation of human skin models that contain rete ridges of controlled geometry would be of great interest for drug testing, disease modeling, and understanding aging effects.

To date, most traditional and bioprinted human skin models consist of a flat interface between the epidermal and dermal layers [11–15]. However, microfabrication methods have recently been used to pattern rete ridges, including stamping [3, 4, 16], laser ablation [5, 17], and casting into molds [18]. Most stamps are limited in depth and lack rounded features. Moreover, human skin models produced using these stamps focus on one cell type and hence do not fully recapitulate the complex 3D microenvironment in native skin [8]. Laser ablation methods can damage cells seeded within the matrices being patterned [5, 17]. Photo-patterning of methacrylated gelatin (GelMA) and poly(ethylene glycol)-diacrylate (PEGDA) has also been explored to create human skin models with rete ridge structures [18]. However, keratinocytes seeded on these extracellular matrices and cultured *in vitro* do not assemble into multilayered epidermis or deposit their own basement membrane [18]. Moreover, it is quite difficult to retain patterned rete ridge structures in skin models due to matrix remodeling and degradation [19].

For example, keratinocytes produce matrix metalloproteinases (MMPs), while fibroblasts and myofibroblasts exert forces that accelerate these deleterious processes [19–28].

Here, we report a micropatterning method to create human skin models replete with rete ridges between their epidermal and dermal layers. Using 3D printed stamps coupled with micromolding, we produced rete ridges composed of rounded features of controlled geometry and periodicity in the dermal layer. We studied the effects of collagen composition and crosslinking on pattern retention during longitudinal culture and found that telocollagen gels crosslinked with 1-ethyl-3-(3-dimethylaminopropyl)carbodiimide (EDC) are resistant to cell-induced degradation. We further observed that epidermal cells seeded on the dermal layer expressed cytokeratins, basement membrane proteins, and proliferation markers. These models, replete with rete ridges, resisted rapid penetration of the cytotoxic benchmark chemical sodium dodecyl sulfate (SDS) [29] and compatibility with keratinocytes from both a neonatal donor and an adult diabetic donor. These 3D-printed stamps offer the potential of a wide range of structures and geometries. Our biomimetic human skin models may find potential application in drug and cosmetic testing, disease modeling, and aging studies.

## 2. Results

### 2.1. Patterning human skin models with rete ridge-like structures

We generated human skin models with rete ridge-like features using silicone stamps (figure 1). The stamps are produced using 3D printed molds that contain a periodic array of ridges of varying height, width, and center-to-center spacing. We implemented a ridged stamp geometry to enable reproducible pattern formation and cross-sectional imaging of the resulting skin models (figure S1), in which the ridge depth ranged from 200 $\mu$m to 500 $\mu$m with center-to-center spacings of 350–500 $\mu$m. Each stamp is manually pressed into the dermis layer, which contains collagen and fibrinogen. In our first model, primary human neonatal dermal fibroblasts are dispersed in the gel, while our second model is stamped without cells, crosslinked, and then seeded with dermal fibroblasts. The stamps rest on the top of 12 well plate Transwell inserts, while contacting a collagen and fibrin pre-gel solution to enable patterning and removal. The stamping process results in undulating features, akin to rete ridges observed in native skin. Fibrin is included in these matrices to increase the pattern fidelity of stamped features. Next, we formed an epidermal layer by seeding primary human keratinocytes on top of the dermal layer. This model is cultured for 4 d in media on a Transwell membrane followed by an additional 10 d at the air–liquid interface to promote the formation of a stratified epidermis. We found that structures stamped in atelocollagen–fibrin matrices quickly collapsed in the presence of keratinocytes and fibroblasts, while telocollagen–fibrin matrices are more robust (figure S2). We therefore used telocollagen–fibrin matrices in our biomimetic human skin models. Without crosslinking the telocollagen–fibrin matrices, rete ridges with slight undulations persist after the 14 day culture period. By contrast, crosslinked telocollagen–fibrin matrices retained much of their original patterned rete ridges over this same period (figures 1(B) and (C)).

Next, we explored the effects of collagen crosslinking and stamp geometry on rete ridge formation in these biomimetic human skin models. When dermal layers composed of telocollagen–fibrin matrices and fibroblasts are seeded with keratinocytes and cultured for 14 d, their patterned rete ridges diminish over time (figures 2 and S3). Skin models patterned with smaller ridges evolved to a nearly flat surface, while those with the larger ridges retained slight undulations that persisted over a 14 day culture period. These features are quantified by their interdigitation index [30], i.e. the ratio of the dermal–epidermal barrier length to the straight-line length. In all cases, the interdigitation index decreased rapidly over the first four days (figures 2(E) and S3). Interestingly, in the absence of keratinocytes, the patterned rete ridges within the dermal layer persisted over this same culture period (figure S4), indicating that keratinocytes play an important role in pattern degradation.

To improve rete-ridge retention, we fabricated a second skin model by crosslinking the stamped telocollagen–fibrin gel with EDC, which has been previously shown to stabilize collagen gels [3–5, 16, 17]. Specifically, we first stamped the telocollagen–fibrin matrix in the absence of dermal fibroblasts, because the crosslinking process will kill fibroblasts encapsulated in this matrix. Next, we crosslinked the gel with EDC and seeded fibroblasts on top of these patterned, crosslinked matrices. Since the fibroblasts are unable to penetrate the crosslinked matrix, they grew on the matrix surface (figures S5(A) and (B)). We allowed the fibroblasts to grow for 4 d (figures S5(C) and (D)) before subsequently seeding the dermal layer with keratinocytes. Using immunofluorescent staining with confocal imaging, we directly observed that the rete-ridge structure persists over the 14 day culture period with keratinocytes (figure 2). We also quantified their interdigitation index as a function of rete-ridge depth and consistently found that crosslinked matrices retained the rete ridge morphology over all feature sizes patterned during this longitudinal period (figures 2(F) and S6). We found that the

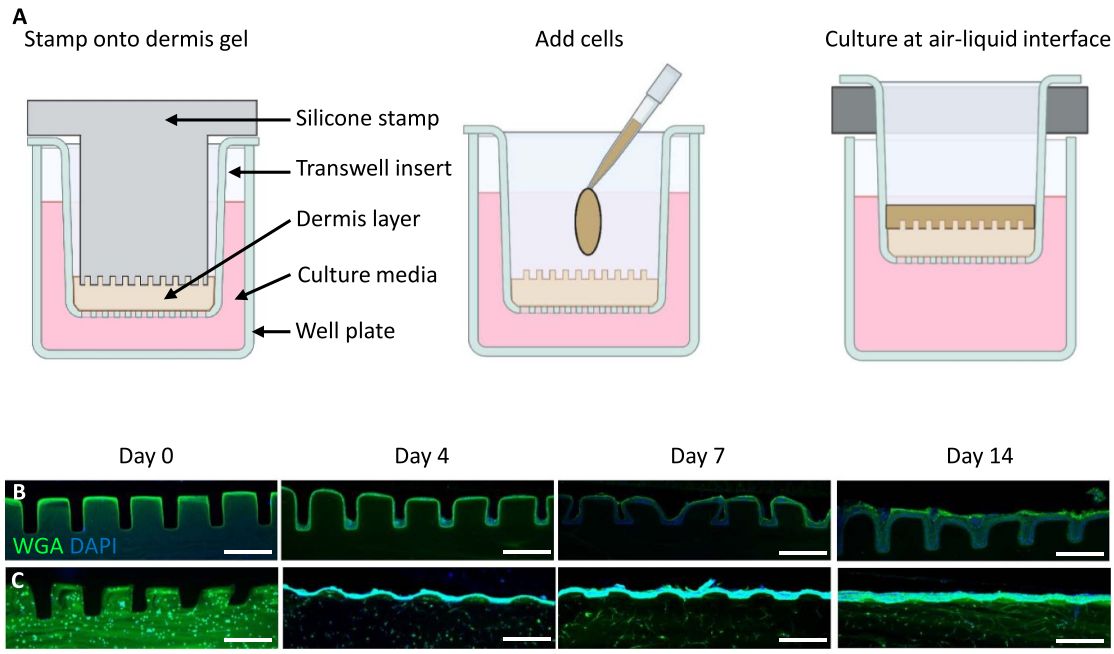


**Figure 1.** Patterning human skin models with rete ridge-like structures. (A) Schematic illustration of the stamping, cell seeding, and longitudinal culture method. (B) Cross-sectional, immunofluorescent images of keratinocytes seeded on EDC-crosslinked, collagen (acellular) layer as a function of culture time (days 0–14) patterned with 500 $\mu$m deep features. (C) Cross-sectional, immunofluorescent images of keratinocytes seeded on a fibroblast-laden, dermal layer (collagen without crosslinks) as a function of culture time (days 0–14) patterned with 500 $\mu$m deep features. Wheat germ agglutinin (green), 4′,6-diamidino-2-phenylindole (DAPI) (blue). Scale bars 500 $\mu$m.

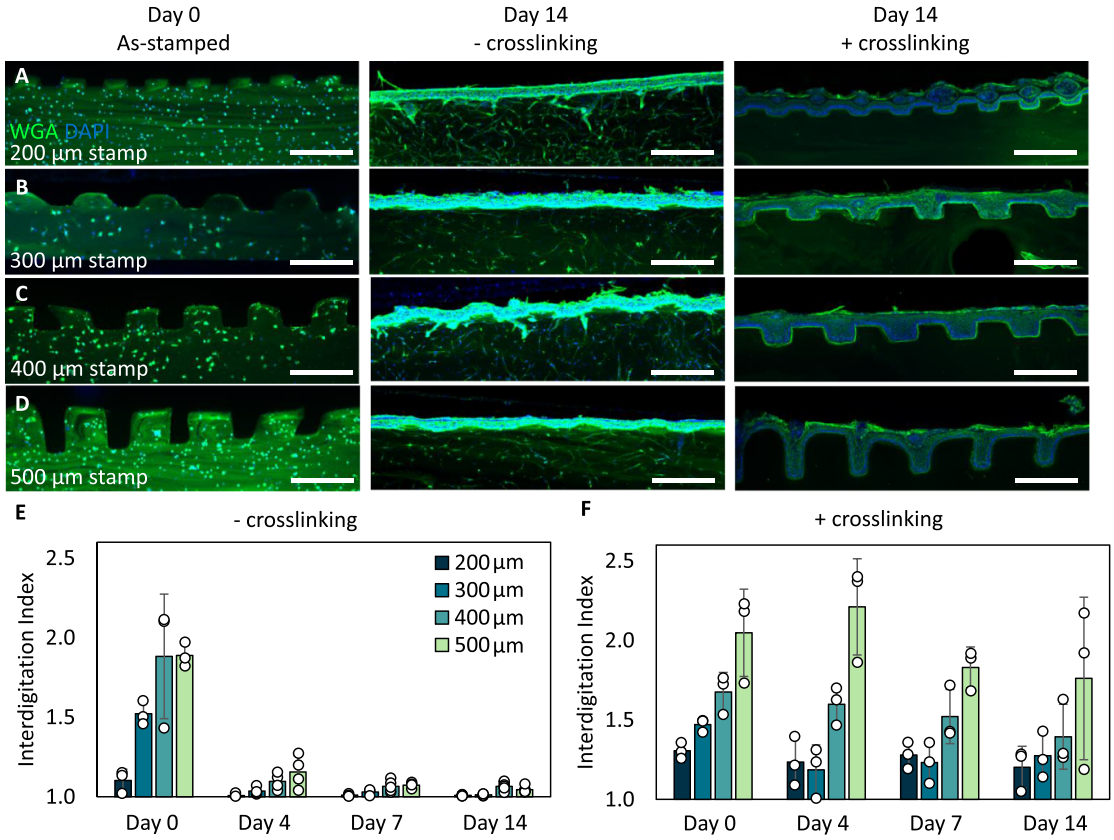


**Figure 2.** Biomimetic human skin models composed of crosslinked matrices retain rete ridge features. (A)–(D) Cross-sectional, immunofluorescent images of skin models at days 0 and 14 with or without EDC crosslinking stamped with: (A) 200 $\mu$m deep features, (B) 300 $\mu$m deep features, (C) 400 $\mu$m deep features, and (D) 500 $\mu$m deep features. (E), (F) Interdigitation index, defined as the length of the dermal–epidermal interface divided by the straight-line distance, as a function of time for all features sizes (E) without crosslinking and (F) with crosslinking. $n = 3$–7. Error bars indicate one standard deviation. Wheat germ agglutinin (green), DAPI (blue). Scale bars 500 $\mu$m.

average epidermal thickness at the final timepoint of the non-crosslinked models was 107 ± 19 $\mu$m and crosslinked models was 163 ± 20 $\mu$m.

### 2.2. Protein expression and basement membrane formation in biomimetic skin models

To evaluate their protein expression, we stained these biomimetic human skin models for cytokeratin 14 and cytokeratin 10, which are expected to be expressed in the basal and suprabasal layers of the epidermis, respectively (figures 3(A) and (E)). In models composed of both crosslinked and non-crosslinked matrices, we observed that cytokeratin 14 expression occurs at the basal layer, while cytokeratin 10 expression occurs in the middle of the epidermis, as expected. We also stained for basement membrane proteins, laminin and collagen IV (Col IV), which are expressed at the interface between the dermal and epidermal layers in both the crosslinked and non-crosslinked matrices (figures 3(B) and (F)). Basement membrane proteins are known to maintain mechanical integrity of human skin when subjected to shear forces [8].

Other studies have reported that markers for epidermal stem cells may be preferentially expressed in the tips or troughs of rete ridges [4, 31–33]. To assess this phenomenon in our biomimetic human skin models, we stained for p63, a putative epidermal stem cell marker [34], and Ki67, a proliferation marker. Both p63 and Ki67 are expressed in the basal layer of the epidermis for both the crosslinked and non-crosslinked models (figures 3(C)–(E) and (H)). This finding is indicative of a functional epidermis, in which basal layer cells actively proliferate, while cells in upper layers lose their ability to proliferate as they undergo keratinization. However, we did not observe a higher density of epidermal stem cells or proliferative cells at the tips of the ridges. Interestingly, we observed spherical growths of proliferative cells in the middle of some of the wells in the EDC-crosslinked samples (figures 2 and 3(E)–(G), day 14 + crosslinking, 200 $\mu$m and 500 $\mu$m). These structures stain brightly for actin (figure 3(E)) and Col IV (figure 3(F)) with many nuclei positive staining positive for p63 (figure 3(G)). We hypothesize that these structures arise due to cell growth inward from the rete ridge walls. However, additional work is needed to elucidate the origin of such architectures.

### 2.3. Adult diabetic human skin model with rete ridges

To demonstrate the generality of our approach, we created a diabetic human skin model composed of primary keratinocytes obtained from an adult diabetic patient, age 70. These cells are seeded on a dermal layer containing fibroblasts in a non-crosslinked telocollagen–fibrin matrix patterned with 400 $\mu$m rete ridges (control) and crosslinked matrices patterned with ridges ranging from 200 $\mu$m to 500 $\mu$m in depth. In all cases, the adult diabetic keratinocytes formed a multilayered, confluent epidermis (figure 4). The interdigitation index for the adult diabetic skin model is significantly lower compared to the models with neonatal keratinocytes patterned with the same ridge depth of 400 $\mu$m (figure 4(F)). However, when adult diabetic donor keratinocytes are cultured on crosslinked matrices, their interdigitation indices are nearly the same as human skin models composed of neonatal keratinocytes (figure 4(G)).

We also investigated whether these adult diabetic human skin models exhibit a differentiated epidermis. As described previously, we stained these models for cytokeratin 10 and 14 (figures 5(A) and (E)). Again, we find that cytokeratin 14 is expressed in the basal layer, while cytokeratin 10 is expressed in the upper layers of the epidermis. When adult diabetic donor keratinocytes are seeded on telocollagen–fibrin matrices without crosslinks, the epidermis layers are thinner compared to those formed using neonatal keratinocytes, which resulted in a lower expression of cytokeratin 10 (figure 5(A)). By contrast using crosslinked matrices, the adult diabetic epidermal layers exhibited a similar thickness as those produced using neonatal keratinocytes with a continuous cytokeratin 10 band forming at the top of each model (figure 5(E)). We also stained for laminin and Col IV to determine whether adult diabetic donor keratinocytes form a basement membrane in these models (figures 5(B) and (F)). We observed similar basement membrane protein production to the neonatal keratinocytes. Finally, we stained these adult diabetic skin models for the proliferative markers, p63 and Ki67 (figures 5(C), (D), (G) and (H)). Akin to models based on neonatal keratinocytes, $p63^+$ and $Ki67^+$ cells line the basal layer of the epidermis. Hence, our adult diabetic human skin models exhibited similar epidermal protein expression patterns to those formed using neonatal keratinocytes.

### 2.4. Biomimetic human skin models are robust

One potential application of these biomimetic human skin models is to study the effects of pharmaceuticals, cosmetics, or occupational hazards on skin *in vitro*. We therefore subjected our models to a common test method for skin irritation [29]. We applied SDS to the top of these skin models after 14 d of culture and then incubated them at 37 °C for 18 h. Upon washing, we measured their cell viability. Models composed of crosslinked matrices seeded with either neonatal or diabetic adult donor keratinocytes exhibited similar cell viability levels after SDS treatment (figure 6), with the latter samples exhibiting slightly lower cell viability at each concentration. Importantly in all cases, these models meet the gold standard of 50% cell viability for this treatment indicating that their epidermal layer inhibits the rapid penetration of SDS.

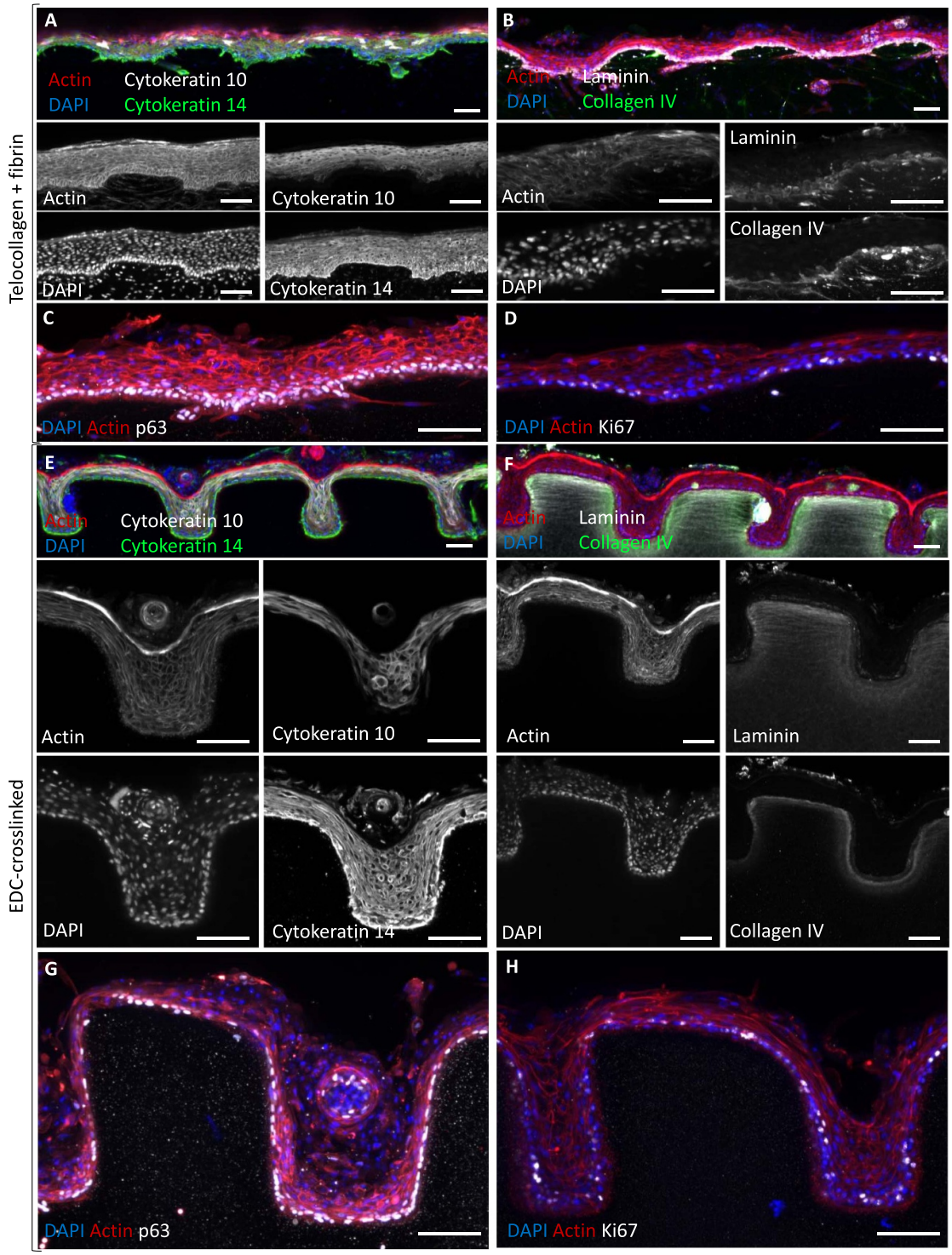


**Figure 3.** Protein expression and basement membrane formation in biomimetic human skin models. (A)–(D) Telocollagen–fibrin skin models. (E)–(H) EDC-crosslinked telocollagen–fibrin skin models. (A) and (E) Cross-sectional immunofluorescent images of cytokeratin 14 (green), cytokeratin 10 (white), actin (red), and DAPI (blue) on biomimetic human skin models at day 14 stamped with 400 $\mu$m deep features. (B) and (F) Cross-sectional immunofluorescent images of collagen IV (green) laminin (white), actin (red), and DAPI (blue) on biomimetic human skin models at day 14 stamped with 400 $\mu$m deep features. (C) and (G) Cross-sectional, immunofluorescent images of p63 (white), actin (red), and DAPI (blue) on biomimetic human skin models at day 14 stamped with 400 $\mu$m deep features. (D) and (H) Cross-sectional, immunofluorescent images of Ki67 (white), actin (red), and DAPI (blue) on biomimetic human skin models at day 14 stamped with 400 $\mu$m deep features. Scale bars = 100 $\mu$m.

### 2.5. Gene expression in biomimetic human skin models

To assess their transcriptional differences, we measured the gene expression of triplicate samples of keratinocytes cultured in a monoculture (without fibroblasts) for 4 days. As a control, neonatal and diabetic adult donor keratinocytes are cultured in 2D to about 80% confluency. Each of these keratinocytes are also cultured on non-patterned and patterned (with 400 $\mu$m rete ridges) telocollagen–fibrin

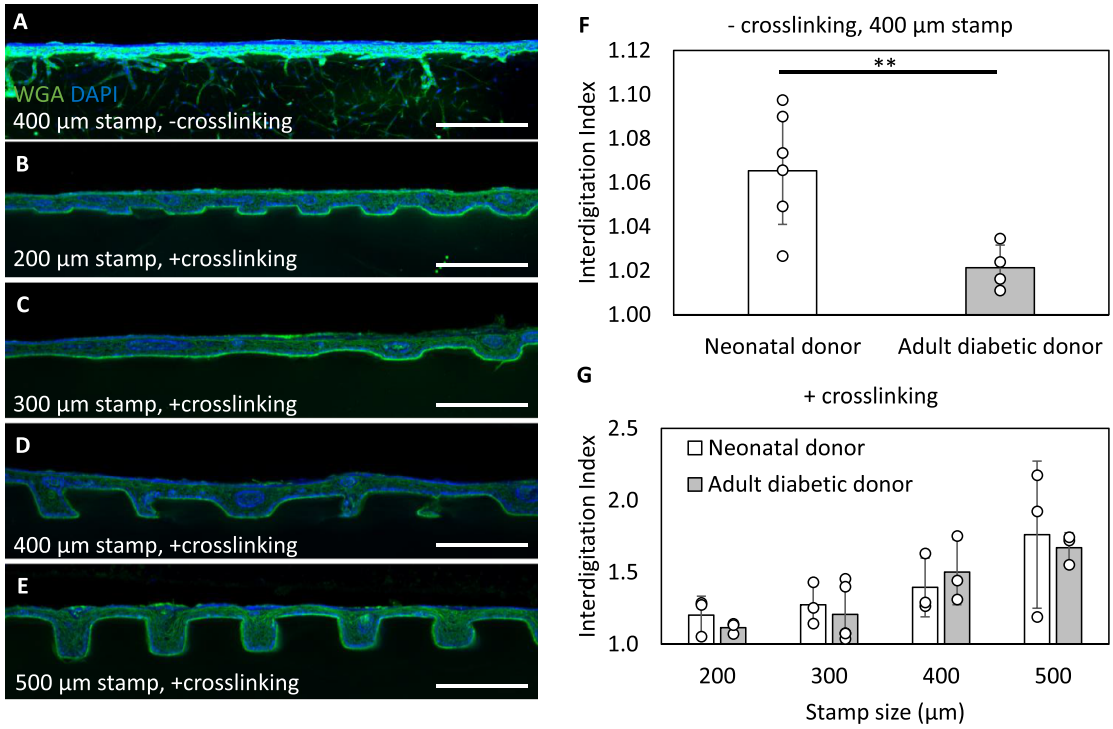


**Figure 4.** Adult diabetic human skin model with rete ridges. (A) Cross-sectional, immunofluorescent image of biomimetic human skin model using adult diabetic donor keratinocytes at day 14 without crosslinking stamped with 400 $\mu$m deep features. (B)–(E) Cross-sectional immunofluorescent images of biomimetic human skin model using adult diabetic donor keratinocytes at day 14 with EDC crosslinking stamped with: (B) 200 $\mu$m features, (C) 300 $\mu$m features, (D) 400 $\mu$m features, and (E) 500 $\mu$m features. (F) Interdigitation index for diabetic donor keratinocytes and neonatal donor keratinocytes cultured on telocollagen–fibrin gel without crosslinking and stamped with 400 $\mu$m deep features. $p = 0.003$ from a two-tailed $t$-test with $n = 4$ for the adult diabetic donor cells and $n = 6$ for the neonatal donor cells. (G) Interdigitation index for adult diabetic and neonatal keratinocytes cultured on stamped and EDC crosslinked telocollagen and fibrin gels. No significant difference was observed between adult diabetic donor and neonatal keratinocytes $p > 0.4$, $n = 3-5$, two-tailed $t$-test. Error bars indicate one standard deviation. Wheat germ agglutinin (green), DAPI (blue). Scale bars 500 $\mu$m.

matrix with and without EDC crosslinker for 4 days. A heatmap of the full data set is provided in figure S7. We focused on differences between neonatal and diabetic adult donor keratinocytes seeded on EDC-crosslinked and stamped telocollagen–fibrin matrices (figures 7(A) and (D)). We observed MMPs are expressed at higher levels in the neonatal keratinocytes, while tissue inhibitor of metalloproteinases 2 (TIMP2) is expressed at a higher level in adult diabetic keratinocytes. Several integrins are also expressed at higher levels in these biomimetic human skin models (a total of 14/60 genes are overexpressed in neonatal keratinocytes, while 11/60 genes were overexpressed in adult diabetic cells). Next, we compared keratinocytes grown in 3D culture on a non-patterned (flat) telocollagen–fibrin matrices to those grown in 2D culture (figures 7(B) and (E)). 10/60 genes are expressed a higher level in 3D culture, while 8/60 genes are expressed higher in 2D culture. Importantly, several integrins are expressed at higher levels in 2D culture, consistent with their role in cell proliferation [35]. These data suggest that some keratinocytes in 3D have already differentiated by day 4. We also find that cadherin-1, a cell-cell adhesion marker, is expressed at higher levels in the 3D model. Interestingly, comparing the gene expression of neonatal keratinocytes grown on flat versus stamped, crosslinked matrices revealed that only 5/60 genes exhibited differences (figures 7(C) and (F)). Hence, the transcriptional differences observed for keratinocytes in 2D versus 3D culture is much larger than those observed between different 3D culture conditions.

## 3. Discussion

We have developed biomimetic human skin models with controlled rete ridges with epidermal and dermal layers on engineered telocollagen–fibrin matrices in the absence and presence of crosslinks. The former models enable fibroblast cells to be readily incorporated in the dermis layer, but patterned rete ridges flatten over time due to the lack of mechanical robustness in the absence of crosslinks. By contrast, the crosslinked models are more durable with patterned rete ridges persisting over longitudinal culture, but lack fibroblasts in the dermal compartment.

Telocollagen gels were shown to be superior to atelocollagen gels in retaining the molded rete ridges. One likely reason why telocollagen degrades more slowly than atelocollagen is that the latter matrix lacks telopeptides, which are known to protect collagen

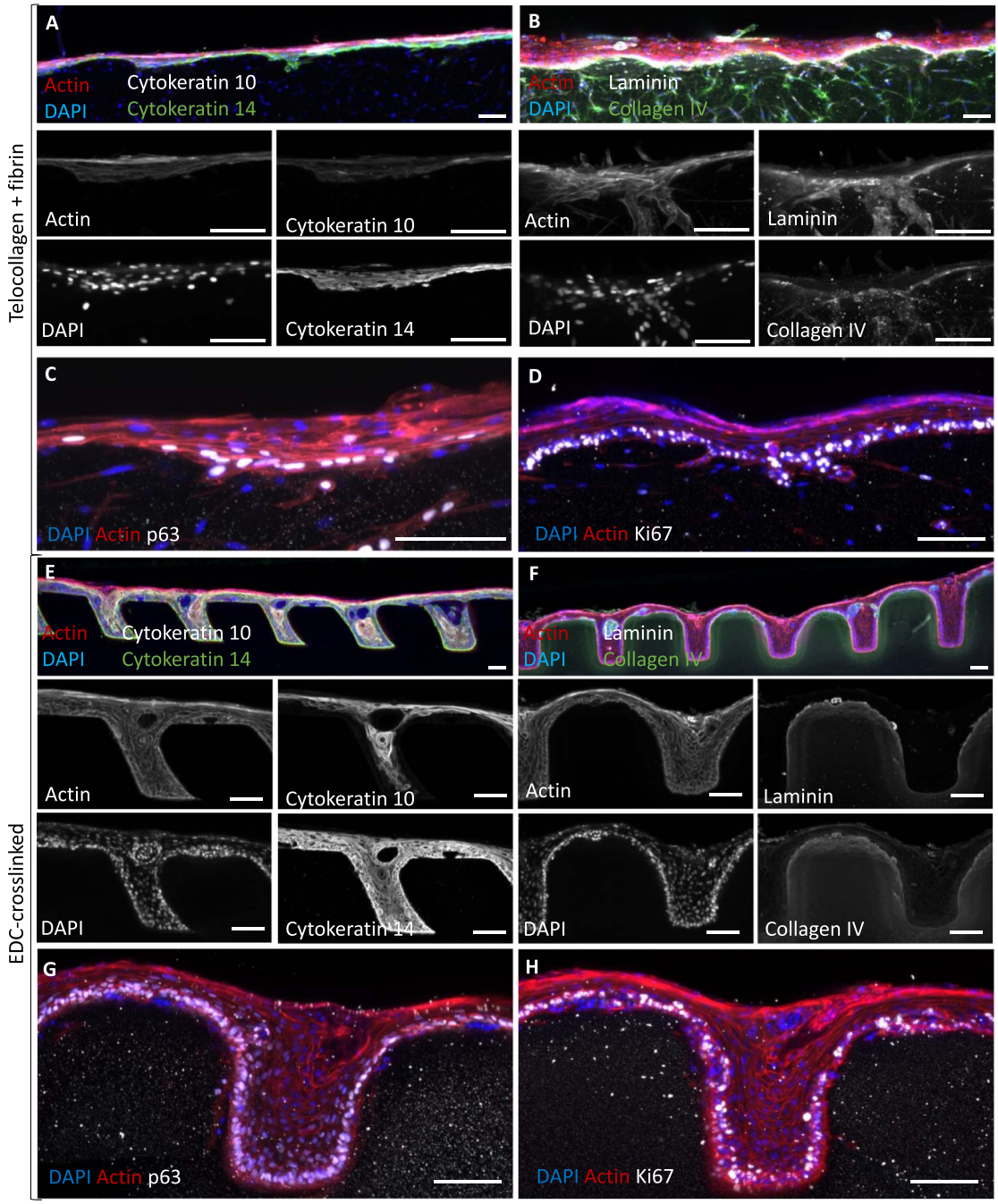


**Figure 5.** Protein expression and basement membrane formation in adult diabetic human skin models. (A)–(D) Telocollagen–fibrin skin models. (E)–(H) EDC-crosslinked telocollagen–fibrin skin models. (A) and (E) Cross-sectional immunofluorescent images of cytokeratin 14 (green), cytokeratin 10 (white), actin (red), and DAPI (blue) on biomimetic human skin models at day 14 stamped with 400 $\mu$m deep features. (B) and (F) Cross-sectional immunofluorescent images of collagen IV (green) laminin (white), actin (red), and DAPI (blue) on biomimetic human skin models at day 14 stamped with 400 $\mu$m deep features. (C) and (G) Cross-sectional, immunofluorescent images of p63 (white), actin (red), and DAPI (blue) on biomimetic human skin models at day 14 stamped with 400 $\mu$m deep features. (D) and (H) Cross-sectional, immunofluorescent images of Ki67 (white), actin (red), and DAPI (blue) on biomimetic human skin models at day 14 stamped with 400 $\mu$m deep features. Scale bars = 100 $\mu$m.

from metalloproteinase cleavage and reduce the rate of collagen degradation [36, 37]. In related work using EDC-crosslinked collagen, researchers have shown that scaffold degradation is reduced [3–5, 16, 17]. Adding fibrin to these collagen matrices enhances gelation initially, which improves the fidelity of the patterned rete ridges.

Other efforts to create patterned human skin models have been confined solely to epidermal layers seeded with keratinocytes [3, 4, 16]. However, fibroblasts play an essential role in the dermis by producing soluble factors that improve keratinocyte differentiation as evidenced by a higher production of basement membrane proteins and a thicker epidermis

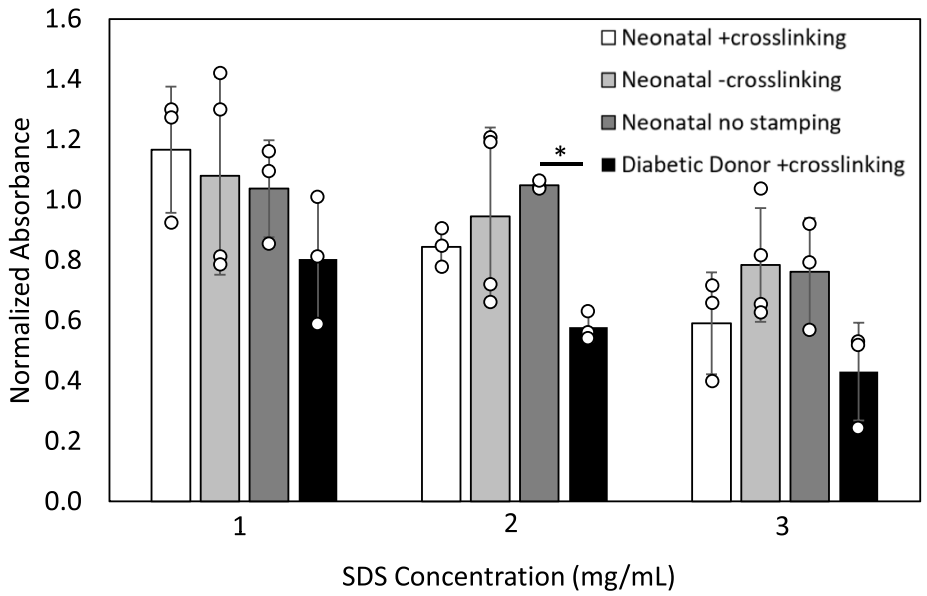


**Figure 6.** Irritation test on biomimetic human skin models. Cell viability as a function of sodium dodecyl sulfate (SDS) concentration introduced on day 14 for an 18 h treatment. Data are normalized to PBS control. Error bars indicate one standard deviation. $n = 3-4$. $^{*}$ $p < 0.05$, for a Tukey's honest significant differences test between the four groups for each concentration.

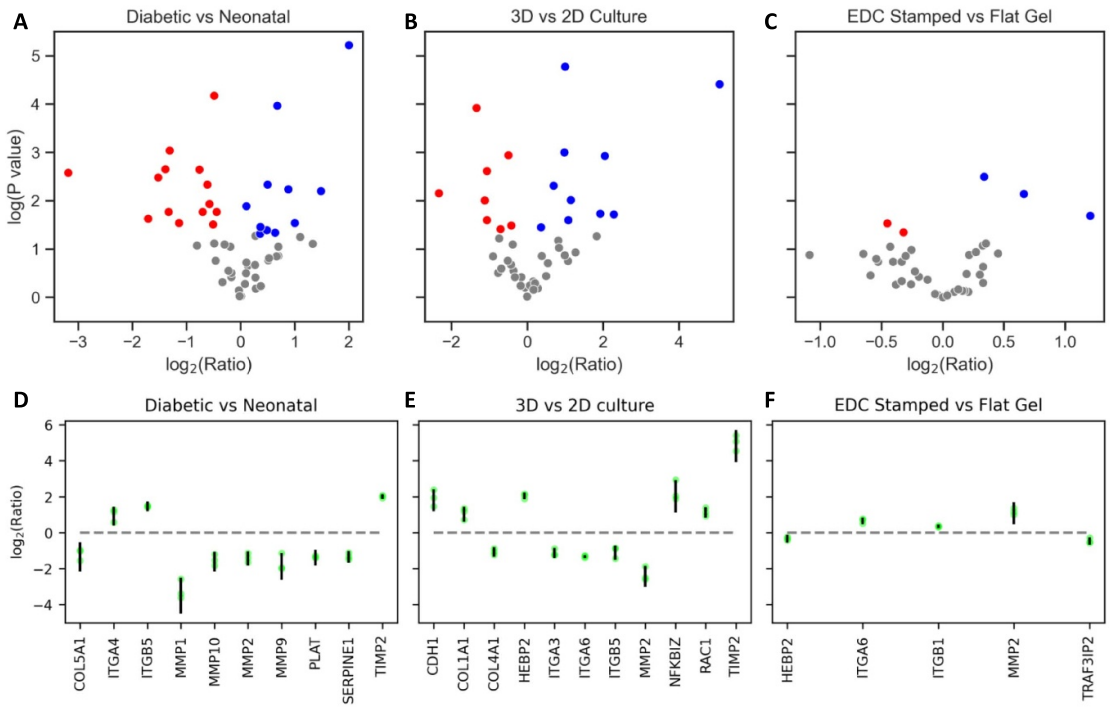


**Figure 7.** Gene expression in biomimetic human skin models. (A) Volcano plot of gene expression comparing neonatal and diabetic adult donor keratinocytes cultured on EDC-crosslinked, patterned telocollagen–fibrin matrices in 3D. Gray dots are genes with $p$ values $> 0.05$, blue dots are genes upregulated in adult diabetic keratinocytes, and red dots are genes upregulated in neonatal keratinocytes. (B) Volcano plot of neonatal keratinocytes cultured on flat telocollagen–fibrin matrices in 3D compared to those cultured in a 2D flask. Gray dots are genes with $p$ values $> 0.05$, blue dots are genes upregulated in 3D culture, and red dots are genes upregulated in 2D culture. (C) Volcano plot of neonatal keratinocytes cultured EDC-crosslinked, patterned and flat telocollagen–fibrin matrices in 3D. Gray dots are genes with $p$ values $> 0.05$, blue dots are genes upregulated in EDC stamped culture, and red dots are genes upregulated in flat gel culture. (D)–(F) Subset of differentially expressed genes ($p < 0.05$) with greatest ratios between (D) adult diabetic donor keratinocytes and neonatal keratinocytes cultured as a monoculture on EDC-crosslinked, patterned telocollagen–fibrin matrix, (E) keratinocytes cultured on a flat telocollagen–fibrin matrix in 3D versus the same cells in 2D culture, and (F) neonatal keratinocytes cultured on an EDC-crosslinked, patterned telocollagen–fibrin matrix in 3D compared to cells grown non-patterned (flat) matrices. In (A)–(C), each dot represents the average of $n = 3$ biological replicates for a particular gene. In (D)–(F), green dots indicate individual biological replicates ($n = 3$), and black bars indicate 95% confidence intervals.

[38]. Other methods, such as laser ablation, yield limited rete ridge or peg geometries and can damage fibroblasts embedded in the matrix [5, 17]. The use of photo-polymerizable GelMA and PEGDA matrices in rete ridge molds have also been explored [18]. Akin to our 3D printed stamping method, their approach enables patterning of rounded rete ridge structures. However, when keratinocytes were cultured on these models *in vitro*, they did not develop a stratified and differentiated epidermis. Rather, the epidermal layer formed consisted of a single layer of keratinocytes located on the tops of their rete ridge structures. Such models would not be expected to resist SDS or other irritant penetration compared to our approach.

Our 3D-printed molds enable rapid development of different stamp geometries that mimic rete ridge structures in different patient subpopulations, e.g. young, old, healthy, and diseased [1, 8–10]. We highlight approaches that generate skin models with modest rete ridges for applications when fibroblasts or other cell types are needed in a separate dermal compartment as well as those with pronounced rete ridges features that are retained over long culture periods. We provide quantitative data regarding the feature degradation over time, which could be applied to other biomimetic human skin models.

Unlike other researchers [4, 31–33], we did not observe different markers for epidermal stem cells localized in the tips or troughs of rete ridges. We posit that this may be due to the lack of endothelial cells pericytes, adipocytes, and other cell types, which are present *in vivo* [6]. We also note that our culture conditions differ from those reported previously, in which keratinocytes were cultured under media for between 1 and 4 d on collagen-coated polydimethylsiloxane (PDMS) substrates [31, 32]. Differences in both culture conditions and substrate stiffness could influence stem cell migration and organization. Our skin models also contained rete ridges, rather than peg-like features demonstrated previously, which may influence stem cell localization [31, 32]. However, 3D printed stamps with peg-like features could be readily generated for future embodiments of these models.

Our ability to generate biomimetic skin models that incorporate adult diabetic keratinocytes may have a potentially important clinical impact, since nearly 40M people in the US alone have this disease. Diabetic patients often exhibit inferior wound healing [39]. Keratinocyte proliferation and migration have been shown to be impaired in diabetes models, but their interactions with immune cells [40], fibroblasts [41], and endothelial cells [42] have not been systematically studied. One limitation of our diabetic skin model is that adult diabetic keratinocytes from 70 year old donor were compared to normal keratinocytes from a neonatal donor. The next generation of biomimetic skin models should be developed using matched cells from healthy and diseased donors and expanded to study other disease states, such as hyperglycemia [43].

In summary, we created a biomimetic human skin model with rete ridges composed of epidermal and dermal layers from both healthy and diseased keratinocytes. We observed the expression of cytokeratins, basement membrane proteins, and proliferation markers. We also carried out irritation tests, which demonstrate that the epidermis inhibits the rapid penetration of SDS, a chemical irritant. Looking ahead, we envision that our biomimetic human skin models may find potential applications in drug and cosmetics testing, disease modeling, and aging studies.

## 4. Methods

### 4.1. Cell culture

Primary human neonatal dermal fibroblasts (ATCC, PCS-201-010), primary human neonatal keratinocytes (ATCC, PCS-200-010), and primary human adult diabetic keratinocytes (Lonza, CC-2926) were used in this study. Fibroblasts were cultured in low-serum fibroblast medium (ATCC, PCS-201-030 and PCS-201-041) and used in experiments from passage number 4–7. Neonatal keratinocytes and adult diabetic keratinocytes were cultured in CnT-Prime medium (CellnTec) and used in experiments from passage number 3–4. All cells were passaged at approximately 80% confluency by washing with phosphate buffered saline (PBS) without calcium and magnesium and adding 0.05% trypsin–EDTA (ethylenediaminetetraacetic acid) for 2–4 min. The trypsin was neutralized using 5% fetal bovine serum (FBS) in PBS without calcium and magnesium. Cells were centrifuged at 150 *g* for 5 min. After passaging, cells were used in experiments or used in continued culture by splitting 1:5 for fibroblasts or 1:3 for keratinocytes.

### 4.2. Silicone stamp fabrication

Molds for silicone stamps were created using an Envisiontec Aureus 3D printer. The printed molds were washed in isopropyl alcohol once for 15 min and then again overnight. After washing, the molds were dried and heated in an oven at 80 °C for 15 min and cured by exposing to UV light for 5 min (Omnicure). Molds were then plasma treated (Diener Zepto-BL-W6) for 5 min and silanized in a vacuum chamber overnight using trichloro(1H,1H,2H,2H-perfluorooctyl)silane. After silanization, the molds were ready for use. Ecoflex 00-50 (Smooth-On) was formulated 1:1 (part A:part B) in a speed mixer at 2000 RPM for 1 min. This mixture was poured into the printed molds and degassed in a vacuum chamber for 10 min. The Ecoflex was then removed from the vacuum chamber and allowed to cure at room temperature for 1 h followed by curing at 80 °C for at least 3 h.

### 4.3. Biomimetic human skin models

Collagen (telocollagen, Advanced Biomatrix TeloCol-10 #5226; atelocollagen, Advanced Biomatrix FibriCol #5133) solutions were prepared by first chilling centrifuge tubes on ice. Second, 10× PBS with phenol red indicator (ATCC, PCS-999-001) was added to the tubes at 1/10 the final volume of solution. Third, 1M NaOH was added to the tubes to neutralize the collagen. Fourth, telocollagen or atelocollagen was added to the tubes after rinsing serological pipettes and pipette tips with ice cold PBS. The collagen was mixed by pipette until the solution color became uniform at a pH of about 7–7.5. If bubbles were introduced during the mixing step, the collagen tubes were centrifuged at 4 °C and 300 *g* for 1 min to remove the bubbles. Collagen tubes were kept on ice until needed for the experiment.

Ecoflex stamps were sterilized by autoclaving and submerged in deionized water. If bubbles were present near the features of the stamps, the autoclaved beaker was briefly sonicated in a water bath until the bubbles were removed (about 10 s). The stamps were removed from the beaker and placed face down in a 24 well plate filled with 2% wt/vol Pluronic F127 (BASF) to coat the silicone in a thin layer of this triblock copolymer. This step reduced the likelihood of bubble formation and prevented the collagen and fibrin gels from sticking to the stamps. The stamps soaked in the 2% Pluronic F127 solution for at least 5 min and then placed in a 24 well plate filled with PBS to soak until needed. The stamps were hydrated by soaking in PBS to reduce the risk of introducing bubbles in biomimetic human skin models during patterning.

Fibrinogen (Millipore, #341573) was prepared in advance by deposition in a 60 mm dish followed by dissolving it in PBS without magnesium and calcium at 37 °C for 2 h at a concentration of 80 mg $ml^{-1}$. The fibrinogen was aliquoted and stored at −20 °C. Prior to experiment, the fibrinogen was thawed and warmed to 37 °C.

Fibroblasts were passaged and counted using Cell Countess (Thermo Fisher). Fibroblasts were split into separate centrifuge tubes so that each sample would have approximately 1–2 million cells $ml^{-1}$. Cells were centrifuged at 150 *g* for 5 min and resuspended briefly in the 80 mg $ml^{-1}$ fibrinogen. Thrombin was added to the collagen solution to a final concentration of 0.5 U $ml^{-1}$, and then the cells in fibrinogen were added to the collagen solution. The final concentrations of all the components were: 7.9 mg $ml^{-1}$ telocollagen or atelocollagen, 4.6 mg $ml^{-1}$ fibrinogen, 0.5 U $ml^{-1}$ thrombin, 1–2 million cells $ml^{-1}$. The pipette tips were rinsed in ice cold PBS before mixing the cells in the collagen solution. 295 $\mu$l of this solution was added to a 12 well plate Transwell insert, and then the Ecoflex stamps were placed on top of the solution. The stamps were designed so that they rested on top of the Transwell inserts while contacting the collagen pre-gel solution. When the 12 well plate was filled with stamped samples, the plate was placed in a 37 °C incubator for 90 min to allow the collagen and fibrinogen to gel. After 90 min, the stamps were removed and CnT–FTAL (full thickness airlift) medium was added on the samples. When the keratinocytes were confluent (either the same day or the next day after preparing the stamped gels), keratinocytes were passaged and added on top of the gels at 400 000 cells per insert.

Samples were then cultured in CnT–FTAL medium for the duration of culture, with media changes every 2–3 d. During the first 4 days of culture, 2 ml of medium was added below the insert, and 0.5 ml of medium was added above the gel. On the fourth day following the addition of keratinocytes, samples were moved to the air–liquid interface by placing a 3 mm silicon rubber spacer below the Transwell® inserts. 2.5 ml of medium was added below the inserts, and any excess medium above the gel was aspirated when samples were treated at the air–liquid interface.

Samples were fixed by removing medium and adding 4% formaldehyde in PBS for 1 h and then washed in PBS three times, 10 min each wash and maintained PBS with 0.05% sodium azide for storage before staining.

For the EDC-crosslinked skin models, collagen solutions and Ecoflex stamp preparation steps were as described above, with the exception that fibroblast cells were not incorporated in the matrix during the stamping process. Thrombin and fibrinogen were added to the collagen solution, which was then pipetted into Transwell® inserts. The stamps were applied on top of the collagen solutions to induce rete ridges. The underlying matrix was then gelled in an incubator at 37 °C for 90 min. After removing the stamps, 2.5 ml of 14 mg $ml^{-1}$ EDC in 100% ethanol was added to each patterned matrix to induce crosslinking. These matrices were crosslinked at room temperature for 24 h and then washed twice in 100% ethanol for 10 min and soaked in 70% ethanol for 24 h. They were then washed in PBS twice for 10 min and soaked in this solution for 24 h. Finally, they were washed once more in PBS and then in CnT–FTAL medium and placed in the incubator to equilibrate before seeding them sequentially with fibroblasts and keratinocytes. Fibroblasts were passaged and seeded at 500 000 cells on each matrix. Fibroblasts were cultured for 4 d on these matrices before adding keratinocytes at 400 000 cells per skin model. The human skin models were cultured as described above, in the same manner as the non-crosslinked samples, using either neonatal or diabetic adult donor keratinocytes.

### 4.4. Irritation test

After keratinocytes had grown for 14 d, 50 $\mu$l of SDS at a concentration between 1 and 3 mg $ml^{-1}$ in PBS was applied to the top of each skin sample. 1× PBS was applied as a negative control. Samples were

incubated with SDS or PBS for 18 h in a 37 °C incubator. Samples in Transwell® inserts were then washed with PBS and moved to a separate 12 well plate with 1 ml of 0.5 mg $ml^{-1}$ 3-(4,5-dimethylthiazol-2-yl)-2,5-diphenyltetrazolium bromide (MTT) in CnT–FTAL media in each well. The MTT viability assay was run for 3 h on a hotplate held at 37 °C. Next, the matrices were removed from the inserts and transferred to a new 12 well plate that contained 2.5 ml of isopropanol per well and soaked for at least 18 h to dissolve the purple formazan substrate. After the substrate was completely dissolved, 50 $\mu$l of isopropanol formazan solution was transferred from each well to a 48 well plate, which was measured on a plate reader using the absorbance setting at 490 nm.

### 4.5. Confocal microscopy

Cross-sections of the biomimetic human skin models were obtained by removing them from the Transwell® inserts and slicing them perpendicular to patterned rete ridges. Samples were cut into small rectangular pieces about 2 mm × 4 mm, which were placed in a 48 well plate for staining. Samples shown in figures 1, 2, 4, S2, S3, S4, and S5 were stained with wheat germ agglutinin at 5 $\mu$g $ml^{-1}$ and 4′,6-diamidino-2-phenylindole (DAPI) at 0.2 $\mu$g $ml^{-1}$ overnight and washed in PBS with 0.05% sodium azide before imaging. While samples shown in figures 3 and 5 were first permeabilized in 0.5% Triton X-100 in PBS for 30 min, then blocked in 5% donkey serum, 0.1% Triton X-100, and PBS overnight followed by incubating with primary antibodies (listed below) for 2–3 d in 5% donkey serum, 0.1% Triton X-100 and PBS. They were then washed three times in PBS for 1 h per wash and incubated with secondary antibodies (listed below), Actin Red 555 ReadyProbes (Thermo Fisher), and DAPI for 1–2 d in 5% donkey serum, 0.1% Triton X-100 and PBS. The samples were then washed three times in PBS for 1 h each wash before imaging on a laser scanning confocal microscope (Zeiss). All primary and secondary antibodies were purchased from Abcam. All primary antibodies were diluted 1:200, and all secondary antibodies were diluted 1:500. Primary antibodies included cytokeratin 10 (rabbit, ab76318), cytokeratin 14 (mouse, ab7800), Ki67 (rabbit, ab15580), p63 (rabbit, ab124762), Col IV (mouse, ab6311), laminin (rabbit ab11575). Secondary antibodies included donkey anti-rabbit IgG H&L Alexa647 (ab150075) and donkey anti-mouse IgG H&L Alexa488 (ab150105).

### 4.6. Image analysis

Images were analyzed using ImageJ. The interdigitation index was measured using the segmented line tool and tracing the boundary between the dermis and epidermis layers of the skin models from one end of the image to the other and comparing to a straight line with the same start and end points. The average thickness was measured using a threshold on the green wheat germ agglutinin channel to identify the epidermis (which was much brighter than the dermis), calculating the area of the epidermis, and dividing the area by the length of the epidermis.

### 4.7. Nanostring gene expression analysis

Monocultures of neonatal keratinocytes and adult diabetic donor keratinocytes were grown on 2D plastic dishes, flat and patterned telocollagen–fibrin matrices with and without EDC-crosslinks. Each sample was prepared as described above with 400 $\mu$m rete ridges, but without fibroblasts. Keratinocytes were seeded on these matrices at 400 000 cells per insert and cultured for four days. RNeasy Mini RNA extraction kits (Qiagen) were used to extract RNA from cells grown on gels. 350 $\mu$l of buffer RLT was pipetted up and down on top of gel for 30 s. Buffer and lysed cells were moved to a tube and the manufacturer protocol was followed to extract RNA. Keratinocytes in 2D culture were passaged at about 80% confluence, centrifuged to a pellet, and the RNeasy manufacturer protocol was followed to extract RNA from these pellets. RNA extracts were stored at −80 °C. Total RNA was quantified using a Nanodrop ND1000 Spectrophotometer (Thermo Fisher Scientific, MA, USA). 75 ng of RNA in 32 $\mu$l total volume was loaded into each lane of an nCounter Sprint Cartridge (NanoString Technologies) as per the manufacturer's instructions. Gene expression was quantified using an nCounter Sprint Profiler (NanoString Technologies). Data were analyzed using Nanostring nSolver 4.0 software, which normalized data to positive controls and six housekeeping genes (ACTB, B2M, GUSB, HPRT1, SDHA, and TBP). The run with adult diabetic donor keratinocytes on a flat gel was removed from the analysis because quality control flags were raised by the nSolver 4.0 analysis software.

## Data availability statement

Data from this study are available on the Materials Data Facility at https://doi.org/10.18126/3A2C-LKAC [44].

## Acknowledgments

The authors thank 3M, Inc. for their generous support of this research and Katharina Kroll and John Ahrens for valuable discussions.

## Author contributions

M B N, S L W, and J A L contributed to the project's inception. All authors contributed to the experimental design. M B N and A J A performed the experiments. All authors provided feedback on experiments and analysis. M B N, A J A, and J A L wrote

the manuscript. All authors provided feedback on the manuscript.

## Conflict of interest

A patent has been filed on this research

## ORCID iDs

Maxwell B Nagarajan https://orcid.org/0000-0003-3207-3282
Jason W Bjork https://orcid.org/0009-0000-7527-7678
Jennifer A Lewis https://orcid.org/0000-0002-0280-2774

## References

[1] Langton A K, Graham H K, McConnell J C, Sherratt M J, Griffiths C E M and Watson R E B 2017 Organization of the dermal matrix impacts the biomechanical properties of skin *Br. J. Dermatol.* **177** 818–27
[2] Woodley D T *et al* 1988 Burn wounds resurfaced by cultured epidermal autografts show abnormal reconstitution of anchoring fibrils *JAMA* **259** 2566–71
[3] Bush K A and Pins G D 2012 Development of microfabricated dermal epidermal regenerative matrices to evaluate the role of cellular microenvironments on epidermal morphogenesis *Tissue Eng.* A **18** 2343–53
[4] Clement A L, Moutinho T J and Pins G D 2013 Micropatterned dermal-epidermal regeneration matrices create functional niches that enhance epidermal morphogenesis *Acta Biomater.* **9** 9474–84
[5] Blackstone B N, Malara M M, Baumann M E, McFarland K L, Supp D M and Powell H M 2020 Fractional $CO_2$ laser micropatterning of cell-seeded electrospun collagen scaffolds enables rete ridge formation in 3D engineered skin *Acta Biomater.* **102** 287–97
[6] Lawlor K and Kaur P 2015 Dermal contributions to human interfollicular epidermal architecture and self-renewal *Int. J. Mol. Sci.* **16** 28098–107
[7] Jones P H, Harper S and Watt F M 1995 Stem cell patterning and fate in human epidermis *Cell* **80** 83–93
[8] Langton A K, Halai P, Griffiths C E M, Sherratt M J and Watson R E B 2016 The impact of intrinsic ageing on the protein composition of the dermal-epidermal junction *Mech. Ageing Dev.* **156** 14–16
[9] Langton A K, Graham H K, Griffiths C E M and Watson R E B 2019 Ageing significantly impacts the biomechanical function and structural composition of skin *Exp. Dermatol.* **28** 981–4
[10] Murphy M, Kerr P and Grant-Kels J M 2007 The histopathologic spectrum of psoriasis *Clin. Dermatol.* **25** 524–8
[11] Cubo N, Garcia M, Del Cañizo J F, Velasco D and Jorcano J L 2016 3D bioprinting of functional human skin: production and *in vivo* analysis *Biofabrication* **9** 015006
[12] Derr K, Zou J, Luo K, Song M J, Sittampalam G S, Zhou C, Michael S, Ferrer M and Derr P 2019 Fully three-dimensional bioprinted skin equivalent constructs with validated morphology and barrier function *Tissue Eng.* C **25** 334–43
[13] Kim B S, Gao G, Kim J Y and Cho D 2019 3D cell printing of perfusable vascularized human skin equivalent composed of epidermis, dermis, and hypodermis for better structural recapitulation of native skin *Adv. Healthcare Mater.* **8** 1801019
[14] Baltazar T *et al* 2020 Three dimensional bioprinting of a vascularized and perfusable skin graft using human keratinocytes, fibroblasts, pericytes, and endothelial cells *Tissue Eng.* A **26** 227–38
[15] Kim B S, Ahn M, Cho W-W, Gao G, Jang J and Cho D-W 2021 Engineering of diseased human skin equivalent using 3D cell printing for representing pathophysiological hallmarks of type 2 diabetes *in vitro Biomaterials* **272** 120776
[16] Suzuki A, Kodama Y, Miwa K, Kishimoto K, Hoshikawa E, Haga K, Sato T, Mizuno J and Izumi K 2020 Manufacturing micropatterned collagen scaffolds with chemical-crosslinking for development of biomimetic tissue-engineered oral mucosa *Sci. Rep.* **10** 1–14
[17] Malara M M *et al* 2020 Cultured epithelial autograft combined with micropatterned dermal template forms rete ridges *in vivo Tissue Eng.* A **26** 0090
[18] Shen Z, Cao Y, Li M, Yan Y, Cheng R, Zhao Y, Shao Q, Wang J and Sang S 2021 Construction of tissue-engineered skin with rete ridges using co-network hydrogels of gelatin methacrylated and poly(ethylene glycol) diacrylate *Mater. Sci. Eng.* C **129** 112360
[19] Shen Z, Sun L, Liu Z, Li M, Cao Y, Han L, Wang J, Wu X and Sang S 2023 Rete ridges: morphogenesis, function, regulation, and reconstruction *Acta Biomater.* **155** 19–34
[20] Parks W C 1999 Matrix metalloproteinases in repair *Wound Repair Regen.* **7** 423–32
[21] Dumin J A, Dickeson S K, Stricker T P, Bhattacharyya-Pakrasi M, Roby J D, Santoro S A and Parks W C 2001 Pro-collagenase-1 (matrix metalloproteinase-1) binds the $\alpha 2\beta 1$ integrin upon release from keratinocytes migrating on type I collagen *J. Biol. Chem.* **276** 29368–74
[22] Krampert M, Bloch W, Sasaki T, Bugnon P, Rülicke T, Wolf E, Aumailley M, Parks W C and Werner S 2004 Activities of the matrix metalloproteinase stromelysin-2 (MMP-10) in matrix degradation and keratinocyte organization in wounded skin *Mol. Biol. Cell* **15** 5242–54
[23] Harris A K, Stopak D and Wild P 1981 Fibroblast traction as a mechanism for collagen morphogenesis *Nature* **290** 249–51
[24] Stopak D and Harris A K 1982 Connective tissue morphogenesis by fibroblast traction: I. Tissue culture observations *Dev. Biol.* **90** 383–98
[25] Rhee S 2009 Fibroblasts in three dimensional matrices: cell migration and matrix remodeling *Exp. Mol. Med.* **41** 858–65
[26] Tomasek J J, Gabbiani G, Hinz B, Chaponnier C and Brown R A 2002 Myofibroblasts and mechano-regulation of connective tissue remodelling *Nat. Rev. Mol. Cell Biol.* **3** 349–63
[27] Karrer S, Bosserhoff A, Weiderer P, Landthaler M and Szeimies R-M 2004 Keratinocyte-derived cytokines after photodynamic therapy and their paracrine induction of matrix metalloproteinases in fibroblasts *Br. J. Dermatol.* **151** 776–83
[28] Martins V L, Caley M and O'Toole E A 2013 Matrix metalloproteinases and epidermal wound repair *Cell Tissue Res.* **351** 255–68
[29] Organization for Economic Cooperation and Development 2021 Test guideline no. 439: *in vitro* skin irritation: reconstructed human epidermis test methods *OECD Guidelines for the Testing of Chemicals, Section 4* (https://doi.org/10.1787/9789264242845-en)
[30] Timár F, Soós G, Szende B and Horváth A 2000 Interdigitation index—a parameter for differentiating between young and older skin specimens *Skin Res. Technol.* **6** 17–20
[31] Mobasseri S A, Zijl S, Salameti V, Walko G, Stannard A, Garcia-Manyes S and Watt F M 2019 Patterning of human epidermal stem cells on undulating elastomer substrates reflects differences in cell stiffness *Acta Biomater.* **87** 256–64
[32] Viswanathan P, Guvendiren M, Chua W, Telerman S B, Liakath-Ali K, Burdick J A and Watt F M 2016 Mimicking the topography of the epidermal-dermal interface with elastomer substrates *Integr. Biol.* **8** 21–29

[33] Connelly J T, Gautrot J E, Trappmann B, Tan D W-M, Donati G, Huck W T S and Watt F M 2010 Actin and serum response factor transduce physical cues from the microenvironment to regulate epidermal stem cell fate decisions *Nat. Cell Biol.* **12** 711–8
[34] Soares E and Zhou H 2018 Master regulatory role of p63 in epidermal development and disease *Cell. Mol. Life Sci.* **75** 1179–90
[35] Watt F M 2002 Role of integrins in regulating epidermal adhesion, growth and differentiation *EMBO J.* **21** 3919–26
[36] Perumal S, Antipova O and Orgel J P R O 2008 Collagen fibril architecture, domain organization, and triple-helical conformation govern its proteolysis *Proc. Natl Acad. Sci.* **105** 2824–9
[37] Shayegan M, Altindal T, Kiefl E and Forde N R 2016 Intact telopeptides enhance interactions between collagens *Biophys. J.* **111** 2404–16
[38] El-Ghalbzouri A, Gibbs S, Lamme E, Van Blitterswijk C and Ponec M 2002 Effect of fibroblasts on epidermal regeneration *Br. J. Dermatol.* **147** 230–43
[39] Baltzis D, Eleftheriadou I and Veves A 2014 Pathogenesis and treatment of impaired wound healing in diabetes mellitus: new insights *Adv. Ther.* **31** 817–36
[40] Piipponen M, Li D and Landén N X 2020 The immune functions of keratinocytes in skin wound healing *Int. J. Mol. Sci.* **21** 8790
[41] Ghahary A and Ghaffari A 2007 Role of keratinocyte–fibroblast cross-talk in development of hypertrophic scar *Wound Repair Regen.* **15** S46–S53
[42] Mercurio L *et al* 2020 Interleukin (IL)-17/IL-36 axis participates to the crosstalk between endothelial cells and keratinocytes during inflammatory skin responses *PLoS One* **15** e0222969
[43] Lan C-C, Liu I-H, Fang A-H, Wen C-H and Wu C-S 2008 Hyperglycaemic conditions decrease cultured keratinocyte mobility: implications for impaired wound healing in patients with diabetes *Br. J. Dermatol.* **159** 1103–15
[44] Nagarajan Maxwell *et al* 2023 Dataset for Biomimetic Human Skin Model Patterned with Rete Ridges, Biofabrication *Materials Data Facility* (https://doi.org/10.18126/3A2C-LKAC)